0031-3998/89/2602-0088$02.00/0
PEDIATRIC RESEARCH

Vol. 26, No. 2, 1989
Printed in U.S.A.

Structural Maturation of the Human Fetal Lung: A Morphometric Study of the Development of Air-Blood Barriers[1]

MARY DiMAIO, JOAN GIL, DOINA CIUREA, AND MEYER KATTAN

Jack and Lucy Clark Department of Pediatrics [M.D., M.K.] and the Lillian and Henry M. Stratton-Hans Popper Department of Pathology [J.G., D.C.], Mount Sinai School of Medicine, New York, New York 10029

ABSTRACT. To quantitatively follow the progressive capillarization of the fetal airway epithelium, we examined human lung tissue from nine fetuses ranging in gestational age from 18–26 wk. Our goals were to *1*) determine the initial time of appearance of the air blood barrier (ABB) in the fetus; *2*) follow the increase in the number of ABB per total epithelial airway surface (capillary load) with gestational age; and *3*) measure the thickness of the ABB. Our results, obtained by using light and electron microscopy and an interactive computerized morphometry system, show that ABB first appear at 19 wk. Increasing gestation is accompanied by an exponential increase in the number of ABB ($r = 0.96$) and the total surface area that the ABB contribute to the total surface area of airway epithelium ($r = 0.93$). ABB thickness is comparable to the dimensions of minimal barrier thickness of the adult ABB. The structural development that we describe may be one of the factors determining preterm viability. (*Pediatr Res* 26: 88–93, 1989)

Abbreviations

ABB, air blood barrier
SDA, total surface density of epithelial airways
VDA, volume density of epithelial airways
SDB, surface density of ABB
CL, capillary load
$\bar{t}$, arithmetic mean thickness of ABB
t_h, harmonic mean thickness of ABB

The mature ABB in mammals is composed of the capillary endothelium, squamous alveolar epithelium, and a narrow interstitial space which in the thinnest area is formed exclusively by the fused basement membranes of the two cell types (1). A key feature of pulmonary maturation is the development of these attenuated areas because they will become the site of optimal gas exchange (1, 2). Indeed, extrauterine survival critically depends on the availability of a structurally efficient gas exchanging apparatus.

It is during the canalicular period of fetal lung development that the first ABB structures appear (3, 4). The canalicular period (17–26 wk) is the time during which the basic acinar structure is established and vascularized (5). The acinus consists of a terminal bronchiole, a series of two to four prospective respiratory bronchioles and a terminal "spray" of six to seven generations of branched buds (5). These airways are lined by columnar or cuboidal epithelium and are surrounded by mesenchyme. Initially, the mesenchyme is poorly vascularized containing few capillaries which are randomly oriented in relation to the epithelial tubules. As the process of canalization progresses, the capillaries rapidly increase in number, appear closer to the airway epithelium, and eventually penetrate between two epithelial cells. This is followed by attenuation of the epithelial lining confined to the area of close apposition of the endothelial and epithelial cells and eventual fusion of both basement membranes (Fig. 1). In this manner, structures comparable to the adult ABB are formed (3, 5, 6). In our study we refer to these thin areas as ABB.

The purpose of our study was to quantitatively follow in weekly intervals the progressive capillarization of the fetal airway epithelium (*i.e.* formation of ABB) in fetuses ranging in gestational age from 18–26 wk. Using light and electron microscopy and an interactive computerized morphometry system, we studied *1*) the initial time of appearance of the ABB in the fetus; *2*) the number of ABB that is present with increasing gestational age; and *3*) we measured the thickness of the ABB in the fetus.

MATERIALS AND METHODS

Materials and lung preparation. Our material consisted of surgically obtained fetal fragments from nine electively terminated normal pregnancies. Approval for the use of fetal tissue was granted by the institutional review board. Based on antenatal clinical evaluation all the fetuses ranged from 18–24 wk gestational age. When gestational age was determined by fetal foot-length (7), a discrepancy of 2 wk was found in two fetuses. Based on the footlength these fetuses were 25–26 wk gestational age.

Within 10 min of fetal demise, a random thin section of lung tissue was taken from one lobe; identification as to its precise anatomic origin was not possible. The lung tissue was immediately fixed in 1.5% glutaraldehyde in 0.1 M cacodylate buffer (pH = 7.3) for 24 h. The tissue was then diced into numerous blocks of 1 mm length, placed in 1.5% osmium tetroxide with S-collidine buffer (pH = 7.4) for 1 h, and then post-fixed in uranyl acetate in maleate buffer (pH = 6) for 45 min. The osmolarity of these solutions was 330 mosmol. After dehydration in graded ethanol, the tissue samples were embedded in Epon 812. Epon 812 does not introduce significant dimensional changes in the tissue (8).

Sampling procedure. Four blocks from each lung specimen were selected at random. For light microscopic study multiple semithin sections of 1 μm were cut per block and stained accord-

Received February 7, 1989; accepted April 26, 1989.
Supported in part by Grant MCJ001069, from the MCH Training Grant, a grant from the United States Department of Health and Human Services, and the National Heart, Lung, & Blood Institute Grant HL34196.
[1] Presented in part at the annual meeting of the American Thoracic Society, Las Vegas, Nevada, May 8, 1988.
Correspondence Dr. M. DiMaio, Mt. Sinai Medical Center, Division of Pediatric Pulmonology, Box 1202, One Gustave L. Levy Place, New York, NY 10029.

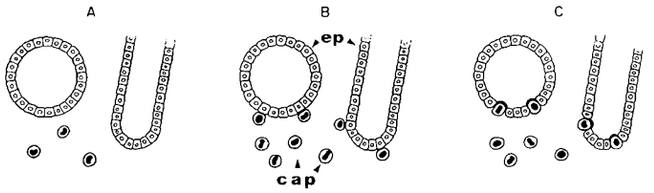

Fig. 1. Longitudinal and cross-sectional drawing of the progressive canalization of the fetal airway epithelium. *A*, the few capillaries present in the mesenchyme are distant and randomly oriented to the epithelium. *B*, capillaries increase in number and appear closer to the epithelium. *C*, capillaries have penetrated between epithelial cells to form air blood barriers against the luminal side of the epithelial tubules. *ep*, epithelium; *cap*, capillary.

ing to Humphrey and Pittman (9). One section was then selected from each block for stereologic measurements.

For electron microscopical examination, ultrathin sections (60–90 nm) were cut with a diamond knife on an LKB ultramicrotome. The sections were mounted on five copper grids and double stained with uranyl acetate and lead citrate (10). Using a JEM CX100 transmission electron microscope, sections from each block were examined for the presence of ABB. We defined these as thin areas of close apposition of the endothelial and epithelial cells accompanied by extreme attenuation of the epithelial lining. (During the canalicular period, the formation of these barriers occurred only along the future airspace. The opposite side of the endothelial cell membrane remained totally within the mesenchyme.) For each block examined, a maximum of 10 fields that contained ABB were selected concomitantly by two observers and photographed at a primary magnification of ×8300. The negatives were then printed at ×2.5 and used for morphometric analysis.

Stereologic methods. We examined the capillarization of the fetal epithelial airway surface with increasing gestational age. Morphometric analysis was performed on an interactive touch screen peripheral overlaid on a monitor displaying the image of the lung tissue from a video camera mounted on a light microscope (11). The projected image was delineated by a rectangular frame generated by the computer thus demarcating a field for study (test area). When a structure contained in the video image is traced, the touch screen transmits the information on the cartesian coordinates of the points activated to the computer, which then stores the points and echoes by generating a white line linking points under the tracing. For example, tracing along the basement membrane of an airway produces a solid line encircling the structure. The tracing is subsequently smoothed, and its length measured by application of the Pythagorean theorem from point to point (11).

Using this system, the following measurements were made by interactive tracing at a magnification of ×40 by a single observer: *1*) SDA; *2*) VDA; *3*) SDB exposed to the airway lumen; *4*) CL defined as the number of ABB per total epithelial airway surface area; and *5*) the ratio of SDB to SDA. Measurements for the SDA and VDA were accomplished by tracing the airways along their basement membrane (perimeter). By tracing along the surface of the ABB exposed to the airway lumen, the SDB was obtained. A total ABB count for the CL was obtained by touching each ABB lining the airway. Calibration of the system was achieved with a stage micrometer before and after measurements were made (11).

The ability to obtain SDA, SDB, and VDA from tracing is founded in basic stereologic relationships (11–13). The length of the boundary line or perimeter (tracing) divided by the test area A (area within the frame) is referred to as the boundary length density BA. This ratio relates to the surface density Sv of the shape being traced.

$$S_v=4\pi \cdot BA$$

The formula shows how tracings are used to study surface densities. The enclosed area of the shape studied divided by the test area A is called the areal density and is identical to the volume density Vv of the shape traced (according to the principle of Delesse) (11).

$$A_A=V_v$$

Thus from length and area measurement, a surface to volume ratio can be derived (11).

$$S/V=4 \cdot B/\pi A$$

Measurements were performed on each of the four lung sections per case except in one case where tissue preservation was not adequate. In this instance only one tissue section was available for study. The entire section was examined for a total of 50.9 ± 16.3 (mean ± SE) fields per case and all pertinent structures falling within the rectangular field were sequentially traced; first, the epithelial surface, second, the differentiated ABB.

The dimensions of the ABB were determined using computerized interactive morphometry based on linear intercept measurements (14). Electron micrographs of the barriers were viewed through a video camera mounted on an illuminated stand. The image was displayed on a monitor overlaid with an interactive touch sensitive screen as previously described. Utilizing a previously described procedure, a grid consisting of four parallel lines is superimposed onto the micrograph (14). The parallel lines permit randomization of the points of sampling for the intercept length measurements and a rectangular frame delineates the test area where sampling occurs. The observer marks the axis of the barrier falling across one of the randomly placed test lines by touching a point on each side of the random line. The computer then generates an orthogonal oriented intercept line (a line perpendicular to the barrier). The length of the intercept crossing from one side of the barrier to the other side is then measured by touching the points of entry and exit. The computer keeps a tally of the number of intercepts made. From the values of the intercept lengths "1i" and "1h", and the total "n" measurements performed, the $\bar{t}$ and t_n mean thickness of the barrier can be estimated (13).

$$\bar{t}=\pi/4 \cdot \sum 1i/n$$
$$t_n=8/3 \cdot 1h$$

The arithmetic mean thickness estimates the tissue mass present per unit of gas exchanging area (1). Mathematical computation of the t_n is weighted in favor of the thin portions of the barrier (1, 8, 15).

Using this method, an acceptable level of accuracy is achieved after only 50 measurements (13). Calibration was accomplished with electron micrographs of a grating replica of 21 600 lines/cm taken at the same magnification used to record barriers. This method was used on each lung section for a total of 22.1 ± 13.71 (mean ± SE) barriers per case and a sum total of 118 ± 76.61 (mean ± SE) measurements per case. All measurements were performed on the barrier surface lining the potential airspace.

The morphometric data for the CL, SDB, and SDA for each case were averaged and the mean CL and SDB/SDA was analyzed by regression analysis for linear and logarithmic fit. These results were expressed as correlation coefficients with footlength and the best fit selected for graphic representation of the data.

The mean for $\bar{t}$ and t_n of each case was calculated. To compare the values obtained for the $\bar{t}$ to the values of the t_n, a paired sample *t*-test was performed.

RESULTS

Descriptive. The lung specimens examined were taken from fetuses ranging in gestational age from 18–26 wk. Light microscopy revealed that by 19–20 wk gestation, capillaries approached the airways and began to penetrate between epithelial cells. ABB

were identifiable at 19–20 wk (Fig. 2). The formation of these barriers occurred only along the future airspace. The opposite side of the endothelial cell membrane remained totally within the mesenchyme. Increasing gestational age was accompanied by a visible increase in barrier numbers bulging into the potential airspace (Fig. 3*A* and *B*). No barriers were seen in the specimen of an 18 week gestation, although only one block of tissue was available for study in this instance.

Electron microscopy confirmed that by 19–20 wk gestation capillaries approached the airway and penetrated between two epithelial cells. This process was noted throughout the canalicular period (Fig. 4 *A* and *B*). The barriers were composed of an attenuated epithelial lining, endothelial lining and an interstitial space containing the basement membranes of the two cell types. Basement membrane fusion was focal and variable in extent and location (Fig. 5*A* and *B*).

An unexpected finding was the presence of the endothelial cell nucleus intercalated within the epithelial and endothelial layers of structures which otherwise resembled air blood barriers (Fig. 6). This was observed in six of the nine fetal lungs and comprised 11% of all the ABB studied.

Morphometry. Analysis of the morphometric data shows that CL and SDB/SDA increase exponentially with increasing foot-length (Figs. 7 and 8). The correlation coefficients for the logarithmic fit were 0.96 and 0.93 for CL and SDB/SDA, respectively. The slopes of the lines were 0.78 for the former and 0.98

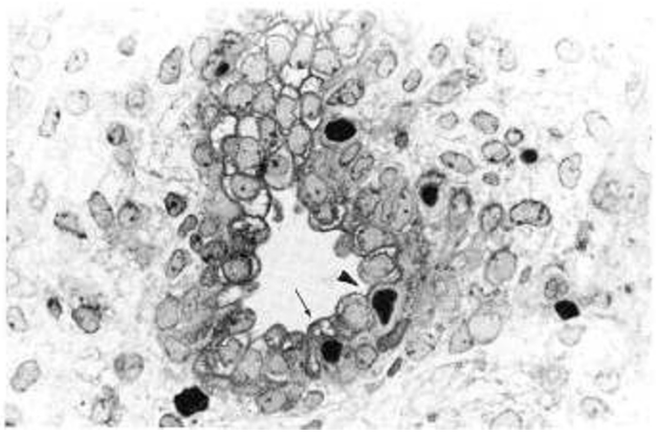

Fig. 2. Photomicrograph (×40) of a microscopic field taken from a fetal lung of 19–20 wk gestation. A capillary is penetrating into the epithelium (*arrow*). An air blood barrier, represented as an area of attenuation of the epithelial lining at the site of close apposition between the endothelial and epithelial cell, is demonstrated (*arrowhead*).

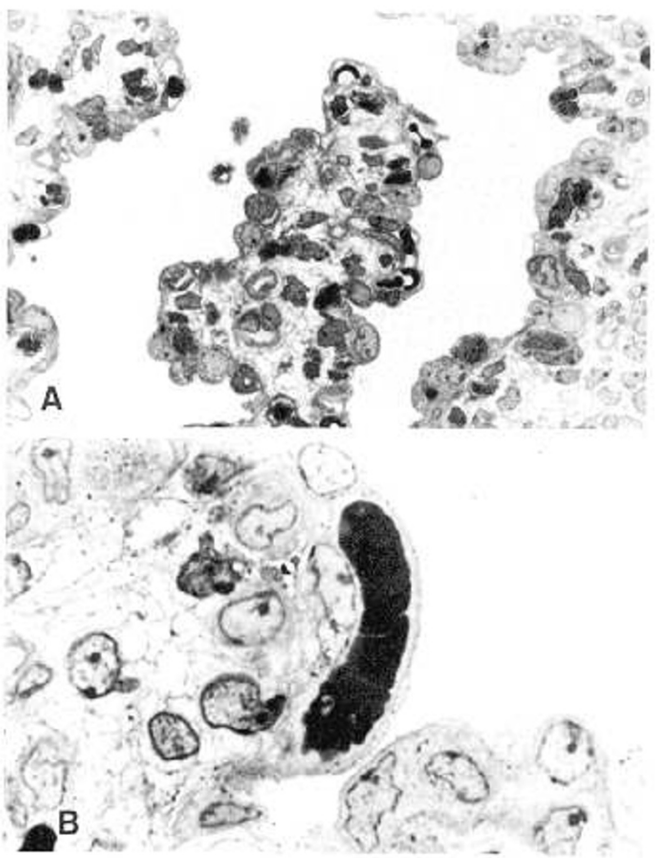

Fig. 3. *A*, photomicrograph (×40) of a microscopic field taken from a fetal lung of 25–26 wk gestation showing increased numbers of air blood barriers lining the potential airspaces. *B*, higher magnification (×100) of one barrier protruding into the potential airspace.

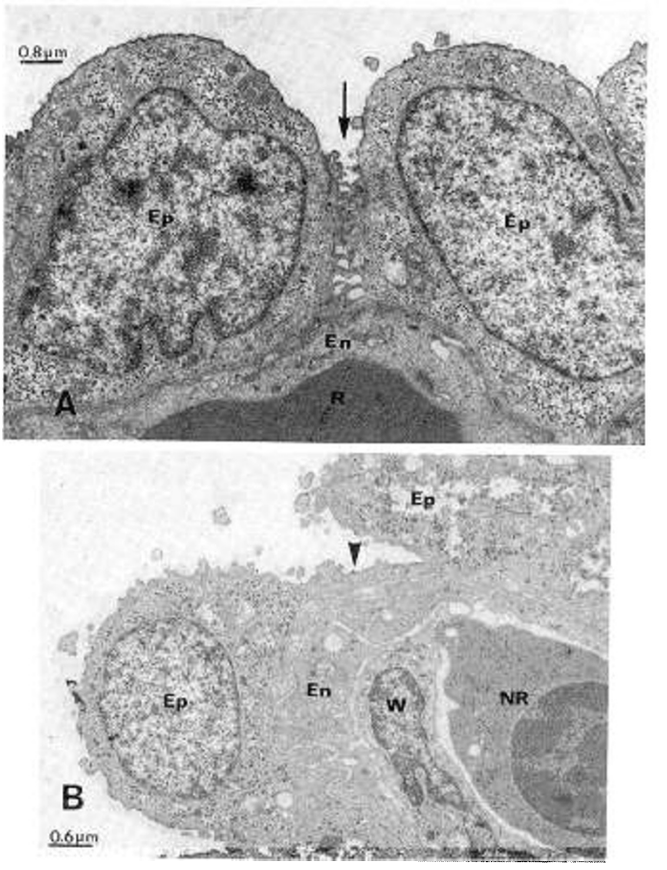

Fig. 4. *A*, electron micrograph (×12,450) of a fetal lung of 24 wk gestation showing a capillary approaching the cuboidal epithelium lining a potential airspace. The endothelial cell appears to be driving a wedge between the epithelial cells (*arrow*). *Ep,* epithelial cell; *En,* endothelial cell; *R*, red blood cell. *B*, electron micrograph (×16,500) of a fetal lung 23–24 wk gestation showing the penetration of the endothelial membrane between two epithelial cells. Attenuation of the epithelial lining has occurred at the area of apposition of the endothelial and epithelial cell. This interface represents an air blood barrier (*arrowhead*). *En,* endothelial cell; *Ep,* epithelial cell; *NR,* nucleated red blood cell; *W*, white blood cell.

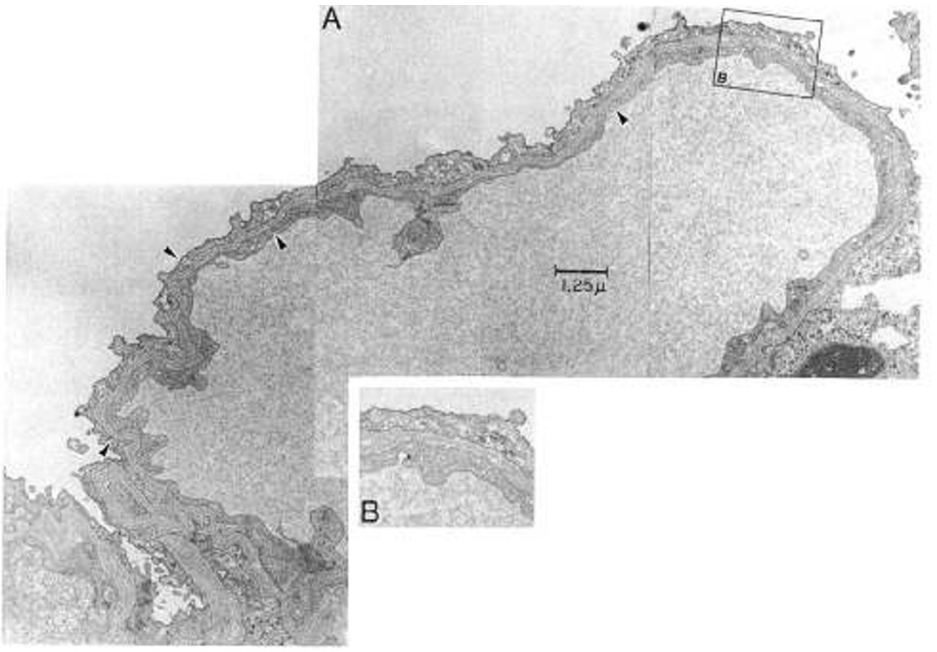

Fig. 5. *A*, montage of four electron micrographs (×20,750) of a single air blood barrier in a fetus 25–26 wk gestation. The barrier is composed of an attenuated epithelial membrane, endothelial membrane, and an interstitial space containing the basement membranes of the two cell types. This appearance is indistinguishable from that of an adult lung photographed at the same magnification. *Arrowheads* indicate areas of fusion between the two basement membranes. *B*, *inset*, higher magnification (×41,500) showing focal basement membrane fusion.

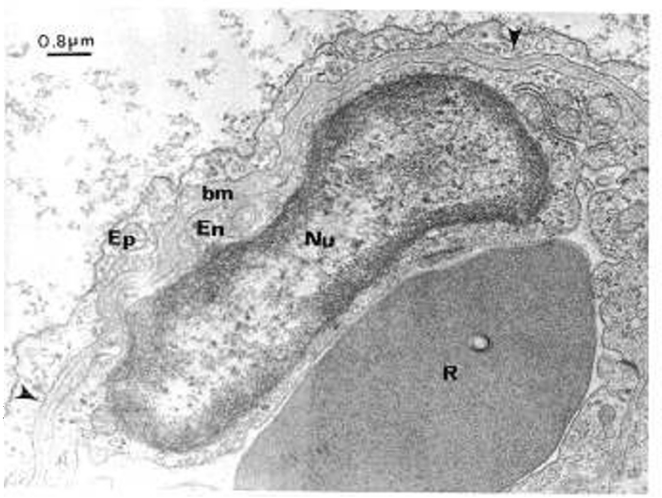

Fig. 6. Electron micrograph (×12,450) of an air blood barrier from a fetus 24 wk gestation showing the intercalation of an endothelial cell nucleus within the barrier. The *arrowheads* indicate points of basement membrane fusion. *En*, endothelial membrane; *Ep*, epithelial membrane; Nu, endothelial cell nucleus; *R*, red blood cell.

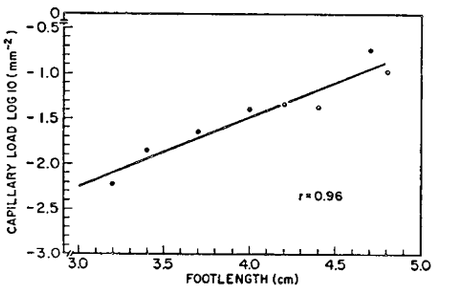

Fig. 7. Logarithmic plot of the capillary load against the fetal footlength. Increasing fetal footlength is accompanied by an exponential increase in the number of air blood barriers per total epithelial airway surface area.

for the latter. Therefore, increasing gestational age (as expressed in footlength) is accompanied by an exponential increase in the number of ABB per unit epithelial surface area and an exponential increase in the total area the barriers contribute to the epithelial airway surface.

With respect to the dimensions of the ABB, the individual mean values for the fetal lungs ranged from 0.28 to 0.53 μm for the t_n and 0.31 to 0.51 μm for the $\bar{t}$. No statistically significant difference was found between t_n and $\bar{t}$ ($p = 0.75$). An average of the means for $\bar{t}$ and t_n was calculated, yielding 0.38 μm ± 0.06

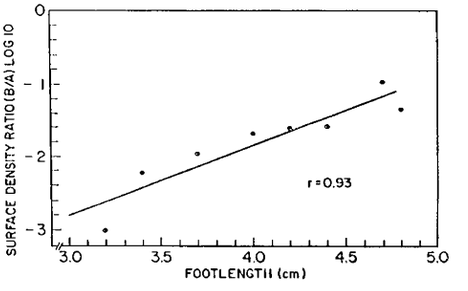

Fig. 8. Logarithmic plot of the ratio of the total surface density of the air blood barriers (*B*) to the total surface density of the airways (*A*) against the fetal footlength. Increasing footlength is accompanied by an exponential increase in the total area the barriers contribute to the epithelial airway surface.

(mean ± SE) for the former and 0.37 μm ± 0.07 (mean ± SE) for the latter.

As previously mentioned, 19 ABB were unique for the presence of the endothelial cell nucleus intercalated within the epithelial and endothelial layers of the barrier. These barriers did not precisely fit our definition of an ABB. Because of this finding, we measured the $\bar{t}$ and t_n of these structures separately and found that the presence of a nucleus increased the thickness by more than 2-fold.

DISCUSSION

In our study we performed a morphometric analysis on human fetal lung tissue to determine the time of appearance and dimensions of the ABB during the canalicular period. In so doing, we have been able to quantitatively follow the capillarization of the developing acinar epithelium and therefore the early development of the lung's gas exchanging surface.

Our morphologic results confirm that during the canalicular period, capillaries approach the epithelial lining of the terminal airways. Air blood barriers appear as areas of extreme epithelial thinning (confined to the area of close apposition of the endothelial and epithelial cell) with sporadic points of fusion between the epithelial and endothelial basement membranes as early as 19–20 wk gestation. These morphologic findings confirm the earlier work of Campiche *et al.* (3) who cited the existence of structures corresponding to the adult ABB at approximately 4 to 5 mo gestation. However, we observed basement membrane fusion by 19 wk gestation, which is earlier than that reported by others (3, 4, 16).

Morphometric analysis demonstrates an exponential relationship between the process of capillarization (represented as the CL) and increasing gestational age. In addition, the total area of ABB integrated into the airway surface also increases exponentially. Therefore, increasing fetal age, as expressed in footlength, is accompanied by an exponential increase in the potential gas exchanging surface.

With respect to ABB dimensions, our findings show that from 19–26 wk gestation, the $\bar{t}$ and t_n of the fetal ABB are less than that of the adult and in most cases equal adult values of minimal barrier thickness (7). The most likely explanation for this finding is that the thinnest portion of ABB form first in fetal development. The morphometric data reflect biologic variability of fetal ABB dimensions. The individual mean values ranged from 0.28 to 0.53 μm for t_n and 0.31 to 0.51 μm for $\bar{t}$. However, we found no statistically significant difference between $\bar{t}$ and t_n, implying that the fetal barrier is uniform in thickness. The values we obtained for ABB thickness contradict the much larger values (1.0 to 1.5 μm) obtained by Campiche *et al.* (3) for barrier thickness. Comparison to our data is difficult because their measurements were confined to only one fetus of 4–5 mo gestation and details as to the method of measuring and sampling size were lacking.

Although the dimensions of the fetal barrier are comparable to the adult, there are structural differences. In the adult barrier each capillary is shared by two alveoli because the capillary is situated between two alveolar surfaces within the interalveolar septum (8). The fetal lung lacks a true interalveolar septum during the canalicular period. Airways of the developing acinus are surrounded by mesenchyme. As capillarization of the epithelium lining the airways progresses, capillaries that participate in the formation of the barrier create a potential gas exchanging surface only along the future airspace. The opposite endothelial side lies totally within the mesenchyme. The observation that the immature alveolar (saccular) septum present in the newborn lung contains a double capillary network (6) can best be explained by understanding that each one of the two epithelial layers contributes its own capillary.

Another difference between the adult and fetal barrier is the extent of basement membrane fusion. In the fetus, barrier basement membrane fusion is focal and variable in length whereas in the adult, nearly one-half of the contact surface between the capillary endothelium and alveolar epithelium is formed exclusively by the fused basement membranes (1). In the adult, the endothelial nucleus is never found in these extremely thin areas. Nuclei are confined to the thick portions of the barrier (where basement membrane fusion does not occur) or intercapillary spaces (2). However, in the fetus we occasionally observed the endothelial nucleus intercalated between the epithelial and endothelial layers of a barrier even in the presence of focal basement membrane fusion.

The notion of fetal lung maturity is often linked to the presence of surfactant materials. Little attention has been paid to structural aspects of maturation particularly at a stage preceding alveolar development. Our work provides data on the progressive capillarization of the developing acinus. The structural development that we describe (*i.e.* the appearance of ABB) may be one of the factors determining preterm viability. Premature infants are handicapped at birth by a large alveolar-arterial shunt, which is believed to be primarily an anatomic intrapulmonary shunt (18). Blood flows through capillaries located in the mesenchymal tissue or through perialveolar vascular rings rather than through the primitive alveoli septa (18, 19). However, extremely premature infants (24–26 wk) may also have reduced capillarization of the airway epithelium contributing to pulmonary underperfusion at these ages.

In support of this possibility, Cater *et al.* (20) recently described two cases of aberrant acinar capillarization which resulted in a syndrome characterized by persistent pulmonary hypertension and severe hypoxemia in the full-term newborn. Morphologically they demonstrated a reduction in the number of capillaries in the acinus and failure of these capillaries to penetrate the alveolar epithelium. The authors concluded that a reduction in the capillary surface area led to increased pulmonary vascular resistance, pulmonary hypertension and hypoxemia.

In summary we conclude *1*) that during fetal lung development ABB appear as focal areas of epithelial thinning and point fusion of the endothelial and epithelial basement membrane as early as 19–20 wk gestation; *2*) there is an exponential relationship between increasing gestational age, CL, and the total surface area that the barriers contribute to the airway surface; and *3*) that the thickness of the ABB is equivalent to adult values of minimal barrier thickness.

We suggest that quantitative criteria for assessing lung maturity and aberrant capillarization of the developing acinus could be established by determining the capillary load in normal and abnormal fetal, preterm, and newborn lungs.

REFERENCES

1. Weibel ER 1973 Morphological basis of alveolar capillary gas exchange. Physiol Rev 53:419–495
2. Weibel ER 1969 The ultrastructure of the alveolar capillary membrane or barrier. In: Fishman AP, Hecht HH (eds) The Pulmonary Circulation and Interstitial Space. University of Chicago Press, Chicago, pp 9–27
3. Campiche MA, Gautier A, Hernandez EI and Reymond A 1963 An electron microscope study of the fetal development of human lung. Pediatrics 32:976–994
4. Gautier A, Campiche M, Bozic C, Hernandez F, Reymond A, Verdon C 1962 Pulmonary epithelium in the human fetus and newborn. In: Breese SS (ed) Electron Microscopy. Proceedings of the 5th International Congress of Electron Microscopy, Philadelphia, PA, pp ww6
5. Boyden EA 1974 The mode of origin of pulmonary acini and respiratory bronchioles in fetal lung. Am J Anat 141:317–328
6. Langston C, Thurlbeck WM 1982 Lung growth and development in late gestation and early postnatal life. Perspect Pediatr Pathol 7:203–235
7. Scammon RR 1937 Two simple nomographs for estimating age and some of the major external dimensions of the human fetus. Anat Rec 68:221–225
8. Weibel ER 1970/1971 Morphometric estimation of pulmonary diffusion capacity I. Model and method. Respir Physiol 11:54–75
9. Humphrey CD, Pittman FE 1974 A simple methylene blue-azure-II-basic

fuchsin stain for epoxy embedded tissue sections. Stain Technol 49:9–14
10. Sato T 1967 A modified method for lead staining of thin sections. J Electron Micros 16:133
11. Gil J, Marchevsky AM, Silage DA 1986 Methods in laboratory investigation. Applications of computerized interactive morphometry in pathology: I. Tracings and generation of graphic standards. Lab Invest 54:222–227
12. Underwood EE 1970 Quantitative Stereology. Addison-Wesley, Reading, MA
13. Weibel ER 1979 Practical Methods of Biological Morphometry. Stereological Methods. Academic Press, London
14. Gil J, Marchevsky AM, Jeanty H 1988 Septal thickness in human lungs assessed by computerized interactive morphometry. Lab Invest 58:466–472
15. Weibel ER 1963 Morphometry of the Human Lung. Springer-Verlag, Heidelberg
16. Groniowski J, Biczyskowa W 1962 Ultrastructure of the blood-air barrier of the neonatal human lungs. In: S. S. Breese (ed) Electron Microscopy. Proceedings of the 5th International Congress of Electron Microscopy Philadelphia, PA, p. ww5.
17. Gehr P, Bachofen M, Weibel ER 1978 The normal human lung: Ultrastructure and morphometric estimation of diffusion capacity. Respir Physiol 32:121–140
18. Hodson WA, Alden ER, Woodrum DE 1977 Gas exchange in the developing lung. In: Hodson WA (ed) Development of the Lung. Marcel Dekker, Inc., New York, pp 469–496
19. Pessacq TP 1972 Considerations on the architectonics of alveolar blood vessels in the lung of the human embryo. Acta Anat 82:118–125
20. Cater G, Thiebeault DW, Beatty EC, Kilbride HW, Huntrakoon M 1989 Misalignment of lung vessels and alveolar capillary dysplasia: A cause of persistent pulmonary hypertension. J Pediatr 114:293–300